# Lecture notes on topological insulators

Ming-Che Chang

*Department of Physics, National Taiwan Normal University, Taipei, Taiwan*

(Dated: January 7, 2021)

**Contents**



## I. EFFECTIVE HAMILTONIAN OF TOPOLOGICAL INSULATOR

During the majority of physical processes, the energy bands far away from the Fermi level remain inert. Therefore, only the energy bands near the Fermi level need be considered. The order of the effective Hamiltonian matrix $\mathsf{H}(\mathbf{k})$ equals the number of bands considered. For example, in the QWZ model, and the BHZ model, 2 bands and 4 bands are considered respectively.

In semiconductors, charge carriers are populated around the minimal energy gap, say at $\mathbf{k}=0$. Therefore, for most purpose, it is sufficient to know the effective Hamiltonian near $\mathbf{k}=0$. Furthermore, since its matrix elements need to respect the symmetry of the system, the form of the effective Hamiltonian is restricted. That is, the symmetry would help us reducing the number of independent parameters.

### A. Symmetry of Hamiltonian

Consider a crystal with point group symmetry $G$. Write the representations for a group element $g\in G$ as $\mathsf{g}$, $\mathsf{U}_g$ (or simply $\mathsf{U}$), and $D_g$ in real space, Hilbert space, and Fock space respectively. Under the action of $g$, an annihilation operator transforms as (Fang *et al.*, 2013),

$$D_g c_\alpha(\mathbf{R}) D_g^{-1} = \sum_{\alpha\beta} U_{\alpha\beta} c_\beta(\mathbf{R}'), \quad \mathbf{R}' = \mathsf{g}\mathbf{R}, \tag{1.1}$$

in which $\alpha,\beta$ are orbital indices, $\mathbf{R}$ is a lattice vector, and $\mathsf{g}$ is a $3\times 3$ matrix of transformation.

Fourier transformation gives

$$c_\alpha(\mathbf{k}) = \frac{1}{\sqrt{N}}\sum_{\mathbf{R}} c_\alpha(\mathbf{R}) e^{-i\mathbf{k}\cdot\mathbf{R}}. \tag{1.2}$$

It transforms as

$$\begin{aligned} D_g c_\alpha(\mathbf{k}) D_g^{-1} &= \frac{1}{\sqrt{N}}\sum_{\mathbf{R}}\sum_{\alpha\beta} U_{\alpha\beta} c_\beta(\mathbf{R}') \underbrace{e^{-i\mathbf{k}\cdot\mathbf{R}}}_{=e^{-i\mathsf{g}\mathbf{k}\cdot\mathbf{R}'}} \\ &= \sum_{\alpha\beta} U_{\alpha\beta} c_\beta(\mathsf{g}\mathbf{k}). \end{aligned} \tag{1.3}$$

Suppose the Hamiltonian is,

$$H = \sum_{\alpha,\beta} H_{\alpha\beta}(\mathbf{k}) c_\alpha^\dagger(\mathbf{k}) c_\beta(\mathbf{k}), \tag{1.4}$$

then the invariance under symmetry transformation requires

$$D_g H D_g^{-1} = H. \tag{1.5}$$

It follows that,

$$\mathsf{U}_g \mathsf{H}(\mathbf{k}) \mathsf{U}_g^{-1} = \mathsf{H}(\mathsf{g}\mathbf{k}). \tag{1.6}$$

### B. Effective Hamiltonian of bulk states

The following discussion is based on Zhang *et al.*, 2009. They focus on materials like $Bi_2Se_3$, $Bi_2Te_3$, and $Sb_2Te_3$ (see Fig. 1). These materials have a layered structure. Each unit cell spans 5 layers stacked along $z$-axis, and there is a three-fold rotation symmetry around the $z$-axis. Each quintuple layer has an inversion center, and these quintuple layers stuck with each other via the Van der Waals force.

We keep only the 4 bands closest to the Fermi level. They are originated from the 4 atomic orbitals $\{|p1_z^+\uparrow\rangle, |p2_z^-\uparrow\rangle, |p1_z^+\downarrow\rangle, |p2_z^-\downarrow\rangle\}$, in which $\pm$ stand for the parities of the states. Therefore, the effective Hamiltonian is a $4\times 4$ matrix. If the orbitals have energies $\varepsilon_0 \pm M_0$, then at the location of minimum energy gap,

$$\mathsf{H}_0 = \mathrm{diag}(\varepsilon_0+M_0, \varepsilon_0-M_0, \varepsilon_0+M_0, \varepsilon_0-M_0). \tag{1.7}$$

As mentioned above, the Hamiltonian is required to satisfy Eq. (1.6). Here the symmetry operators are:
TR:

$$\Theta = i\sigma_y K \otimes 1 = \begin{pmatrix} 0 & 0 & 1 & 0 \\ 0 & 0 & 0 & 1 \\ -1 & 0 & 0 & 0 \\ 0 & -1 & 0 & 0 \end{pmatrix} K, \tag{1.8}$$

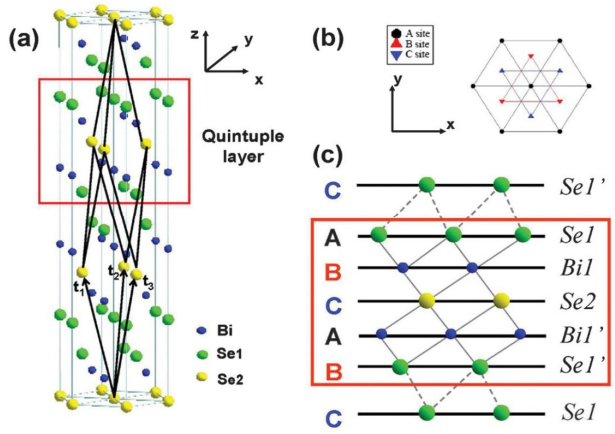


FIG. 1 (a) Crystal structure of $Bi_2Se_3$. (b) Top view of the (111)-surface. (c) Side view of the layered structure. Fig from Qi and Zhang, 2011.

SI:

$$\Pi = 1 \otimes \tau_z = \begin{pmatrix} 1 & 0 & 0 & 0 \\ 0 & -1 & 0 & 0 \\ 0 & 0 & 1 & 0 \\ 0 & 0 & 0 & -1 \end{pmatrix}, \tag{1.9}$$

Rotation:

$$C_3 = e^{i\frac{\pi}{3}\sigma_z} \otimes 1 = \begin{pmatrix} e^{i\pi/3} & 0 & 0 & 0 \\ 0 & e^{i\pi/3} & 0 & 0 \\ 0 & 0 & e^{-i\pi/3} & 0 \\ 0 & 0 & 0 & e^{-i\pi/3} \end{pmatrix}. \tag{1.10}$$

The Pauli matrices $\boldsymbol{\sigma}$ and $\boldsymbol{\tau}$ stand for spin and orbital degrees of freedom.

Let $\mathsf{h}_{ij}(\mathbf{k})$, $i,j = 1,2$, be the $2\times 2$ submatrices of $\mathsf{H}(\mathbf{k})$. Inversion symmetry requires

$$\Pi \mathsf{H}(\mathbf{k}) \Pi^{-1} = \mathsf{H}(-\mathbf{k}). \tag{1.11}$$

That is,

$$\tau_z \mathsf{h}_{ij}(\mathbf{k}) \tau_z = \mathsf{h}_{ij}(-\mathbf{k}). \tag{1.12}$$

Or,

$$\begin{pmatrix} a_{11} & -a_{12} & a_{13} & -a_{14} \\ -a_{21} & a_{22} & -a_{23} & a_{24} \\ a_{31} & -a_{32} & a_{33} & -a_{34} \\ -a_{41} & a_{42} & -a_{43} & a_{44} \end{pmatrix}_{\mathbf{k}} = \begin{pmatrix} a_{11} & a_{12} & a_{13} & a_{14} \\ a_{21} & a_{22} & a_{23} & a_{24} \\ a_{31} & a_{32} & a_{33} & a_{34} \\ a_{41} & a_{42} & a_{43} & a_{44} \end{pmatrix}_{-\mathbf{k}}. \tag{1.13}$$

So $a_{11}, a_{13}, \cdots$ are even in $\mathbf{k}$, $a_{12}, a_{14}, \cdots$ are odd in $\mathbf{k}$.

Three-fold rotation symmetry requires

$$C_3 \mathsf{H}(\mathbf{k}) C_3^{-1} = \mathsf{H}(e^{\mp i2\pi/3} k_\pm, k_z), \tag{1.14}$$

where $k_\pm \equiv k_x \pm i k_y$. The LHS is

$$C_3 \mathsf{H}(\mathbf{k}) C_3^{-1} = \begin{pmatrix} \mathsf{h}_{11} & e^{i2\pi/3}\mathsf{h}_{12} \\ e^{-i2\pi/3}\mathsf{h}_{21} & \mathsf{h}_{22} \end{pmatrix}_{\mathbf{k}}, \tag{1.15}$$

where $\mathsf{h}_{21} = \mathsf{h}_{12}^\dagger$. Therefore, up to quadratic power, $\mathsf{h}_{11}, \mathsf{h}_{22}$ can only have $k_z, k_+k_- = k_x^2 + k_y^2 (\equiv k_\perp^2)$, and $k_z^2$; $\mathsf{h}_{12}$ can only have $k_-^1$.

Time reversal symmetry requires

$$\Theta \mathsf{H}(\mathbf{k}) \Theta^{-1} = \mathsf{H}(-\mathbf{k}). \tag{1.16}$$

The LHS is

$$\Theta \mathsf{H}(\mathbf{k}) \Theta^{-1} = \begin{pmatrix} \mathsf{h}_{22}^* & -\mathsf{h}_{12}^T \\ -\mathsf{h}_{12}^* & \mathsf{h}_{11}^* \end{pmatrix}_{\mathbf{k}}, \tag{1.17}$$

Therefore,

$$\mathsf{h}_{11}(\mathbf{k}) = \mathsf{h}_{22}^*(-\mathbf{k}), \tag{1.18}$$
$$\mathsf{h}_{12}(\mathbf{k}) = -\mathsf{h}_{12}^T(-\mathbf{k}). \tag{1.19}$$

Combine these 3 symmetries, one has

$$\mathsf{H}(\mathbf{k}) = \varepsilon_0(\mathbf{k}) + \begin{pmatrix} M(\mathbf{k}) & A_1 k_z & 0 & A_2 k_- \\ A_1 k_z & -M(\mathbf{k}) & A_2 k_- & 0 \\ 0 & A_2 k_+ & M(\mathbf{k}) & -A_1 k_z \\ A_2 k_+ & 0 & -A_1 k_z & -M(\mathbf{k}) \end{pmatrix}, \tag{1.20}$$

where

$$M(\mathbf{k}) = M_0 - B_1 k_z^2 - B_2 k_\perp^2, \tag{1.21}$$
$$\varepsilon_0(\mathbf{k}) = \varepsilon_0 + D_1 k_z^2 + D_2 k_\perp^2. \tag{1.22}$$

The undetermined parameters need be fit with the actual energy dispersion near the energy gap.

If the basis are arranged in the order of $\{|p1_z^+ \uparrow\rangle, |p2_z^- \downarrow\rangle, |p1_z^+ \downarrow\rangle, |p2_z^- \uparrow\rangle\}$, then

$$\mathsf{H}(\mathbf{k}) = \varepsilon_0(\mathbf{k}) + \begin{pmatrix} M(\mathbf{k}) & A_2 k_- & 0 & A_1 k_z \\ A_2 k_+ & -M(\mathbf{k}) & -A_1 k_z & 0 \\ 0 & -A_1 k_z & M(\mathbf{k}) & A_2 k_+ \\ A_1 k_z & 0 & A_2 k_- & -M(\mathbf{k}) \end{pmatrix}. \tag{1.23}$$

This can be obtained by first exchanging the 2nd and the 4th columns, followed by exchanging the 2nd and 4th rows of the $\mathsf{H}$ in Eq. (1.20). If $A_1 = 0$, then this reduces to a block-diagonal Hamiltonian, similar to the 2D BHZ Hamiltonian.

### C. Effective Hamiltonian of TI surface states

Similar to the TI bulk-state Hamiltonian, one can deduce the effective Hamiltonian for the surface states based on the consideration of symmetry. As an example, we consider the [111] surface state of $Bi_2Te_3$ (see Fig. 1(b)). In addition to the TRS, there is also a $C_{3v}$ symmetry, which consists of a 3-fold rotation transformation $C_3$ and a mirror transformation $M : x \to -x$.

The operator for the 3-fold rotation is

$$C_3 = e^{i\pi/3\sigma_z}. \tag{1.24}$$

The mirror operation $M$ needs to flip the signs of $\sigma_y, \sigma_z$, but preserve the sign of $\sigma_x$. Note that a mirror reflection

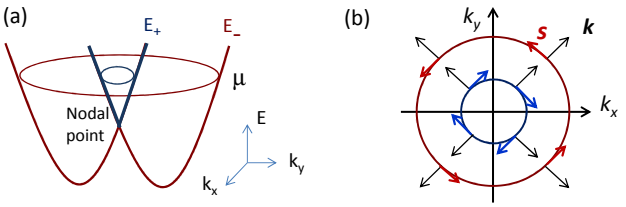


FIG. 2 (a) The energy dispersion of the Rashba system consists of two paraboloids. The magnitude of $\alpha$ is highly exaggerated in the figure. (b) When the chemical potential $\mu$ is above the nodal point, there are two Fermi circles. The spin of an electron follows the direction of the effective magnetic field $\mathbf{b}(\mathbf{k}) = \alpha\mathbf{k}\times\hat{z}$, which is always perpendicular to the momentum.

in 3D equals an inversion followed by a 180° rotation. Therefore, $M^2 = -1$ for spin-1/2 electron (Kane, 2013). These restrictions give

$$M = i\sigma_x \tag{1.25}$$

The effective Hamiltonian is transformed as ($\Theta = i\sigma_y K$),

$$\Theta\mathsf{H}(\mathbf{k})\Theta^{-1} = \mathsf{H}(-\mathbf{k}), \tag{1.26}$$
$$C_3\mathsf{H}(k_\pm)C_3^{-1} = \mathsf{H}(e^{\mp i2\pi/3}k_\pm), \tag{1.27}$$
$$M\mathsf{H}(k_\pm)M^{-1} = \mathsf{H}(-k_\mp), \tag{1.28}$$

where $\mathbf{k} = (k_x, k_y)$. Write the $2\times 2$ Hamiltonian matrix as

$$\mathsf{H}(\mathbf{k}) = \begin{pmatrix} h(\mathbf{k}) & g(\mathbf{k}) \\ g^*(\mathbf{k}) & -h(\mathbf{k}) \end{pmatrix}, \tag{1.29}$$

then time-reversal symmetry dictates that $h(-\mathbf{k}) = -h(\mathbf{k}), g(-\mathbf{k}) = -g(\mathbf{k})$.

Rotation symmetry gives

$$h(k_\pm) = h(e^{\mp 2\pi i/3}k_\pm); \tag{1.30}$$
$$e^{i2\pi/3}g(k_\pm) = g(e^{\mp 2\pi i/3}k_\pm). \tag{1.31}$$

Mirror symmetry gives

$$h(k_\pm) = -h(-k_\mp); \tag{1.32}$$
$$g(k_\pm) = g^*(-k_\mp). \tag{1.33}$$

To linear order of the momentum, it is not difficult to see that $h(\mathbf{k}) = 0, g(\mathbf{k}) = ik_-$. Therefore,

$$\mathsf{H}(\mathbf{k}) = \varepsilon_0(k) + v(\sigma_x k_y - \sigma_y k_x). \tag{1.34}$$

To the third order of momentum, it is left as an exercise to show that

$$\mathsf{H}(\mathbf{k}) = \varepsilon_0(k) + v_k(\sigma_x k_y - \sigma_y k_x) + \frac{\lambda}{2}\left(k_+^3 + k_-^3\right)\sigma_z, \tag{1.35}$$

where $v_k = v_0(1+\alpha k^2)$. The energy dispersion is

$$\varepsilon_\pm(\mathbf{k}) = \varepsilon_0(k) \pm \sqrt{v_k^2 k^2 + \lambda^2 k^6\cos^2(3\theta)}, \tag{1.36}$$

where $\theta = \angle(\mathbf{k}, \hat{x})$. This would give a Fermi contour with 6-fold rotation symmetry (Fu, 2009), which is consistent with observation (Xu *et al.*, 2011).

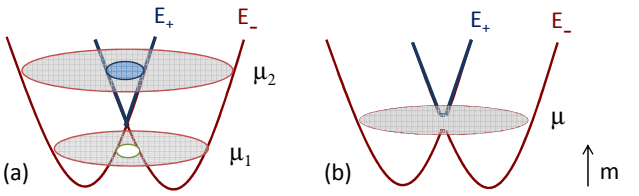


FIG. 3 Fig. (a) shows the Fermi circles for chemical potential lower ($\mu_1$), or higher ($\mu_2$), than the nodal energy. In Fig. (b), the nodal point is lifted by magnetization, and the chemical potential is within the energy gap.

### D. Berry curvature near level crossing

In the following, we review several systems with nodal points in energy spectrum: Rashba system, graphene, and the surface state of 3D TI. They are all 2D systems. Near a nodal point, the system can be approximated as a two-level system (assuming there is no spin degeneracy), and the effective Hamiltonian can be expanded by Pauli matrices. Nodal points in 3D systems will be investigated in the chapters on Weyl semimetal.

#### 1. Rashba system

For the 2DEG in an asymmetric quantum well, there can be **Rashba spin-orbit coupling** (Bihlmayer *et al.*, 2015). The Hamiltonian is,

$$\mathsf{H}(\mathbf{k}) = \frac{\hbar^2k^2}{2m^*} + \alpha\left(\boldsymbol{\sigma}\times\mathbf{k}\right)\cdot\hat{z}, \tag{1.37}$$

where $\alpha$ is the strength of the Rashba coupling, and $z$ is the direction perpendicular to the 2DEG. The energy spectrum is,

$$E_\pm = \frac{\hbar^2k^2}{2m^*} \pm \alpha k, k = |\mathbf{k}|. \tag{1.38}$$

They are two paraboloids with a point degeneracy at $k = 0$.

When the chemical potential is above the nodal point, there are two Fermi circles, see Fig. 2(a). When written in the standard form,

$$\mathsf{H}(\mathbf{k}) = \frac{\hbar^2k^2}{2m^*} + \mathbf{b}(\mathbf{k})\cdot\boldsymbol{\sigma}, \tag{1.39}$$

the Rashba coupling acts like a $\mathbf{k}$-dependent magnetic field, $\mathbf{b}(\mathbf{k}) = \alpha\mathbf{k}\times\hat{z} = \alpha(k_y, -k_x, 0)$. The spins of the electrons on the Fermi circles are parallel or anti-parallel to the effective magnetic field $\mathbf{b}(\mathbf{k})$, see Fig. 2(b).

After circling the Fermi circle once, an electron acquires a Berry phase proportional to the solid angle $\Omega_C$ extended by the spin vector,

$$\gamma_\pm = \mp\frac{1}{2}\Omega_C. \tag{1.40}$$

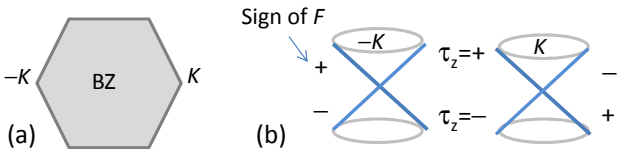


FIG. 4 (a) Brillouin zone of graphene, with valleys $K$ and $-K$. (b) Dirac cones at the two valleys. Valence band has $\tau_z = -$, and conduction band has $\tau_z = +$. The signs of the Berry curvatures for the conduction bands and the valence bands are indicated.

Since the spin always lies on a plane, the solid angle is $2\pi$, and the Berry phases are $\gamma_\pm = \mp\pi$.

The value of the Berry phase remains to be $\pi$, irrespective of the size of the Fermi circle, as long as the path $C$ encloses the nodal point. This implies that the Berry curvature is a delta function,

$$F_z^\pm(\mathbf{k}) = \mp\pi\delta^2(\mathbf{k}). \tag{1.41}$$

The Hall conductivity is given as,

$$\sigma_H = \frac{e^2}{h}\frac{1}{2\pi}\left(\int_{\text{filled}} d^2k F_z^+ + \int_{\text{filled}} d^2k F_z^-\right). \tag{1.42}$$

Since the two branches of the paraboloids have Berry curvatures with opposite signs. Therefore, when the chemical potential $\mu$ is higher than the nodal energy, the two integrals of Berry curvature cancel with each other. If $\mu$ is below the nodal energy, then the Fermi sea does not enclose the node (see Fig. 3(a)), and the two integrals are both zero. Therefore, no matter where $\mu$ is, the Hall conductivity is zero.

If the 2DEG is doped with magnetization $m$, then

$$\mathsf{H}(\mathbf{k}) = \frac{\hbar^2k^2}{2m^*} + \alpha\left(\boldsymbol{\sigma}\times\mathbf{k}\right)\cdot\hat{z} + m\sigma_z. \tag{1.43}$$

The magnetization opens a gap at the node, see Fig 3(b). The Berry curvature becomes (Culcer *et al.*, 2003),

$$F_z^\pm(\mathbf{k}) = \mp\frac{\alpha^2 m}{2(m^2+\alpha^2k^2)^{3/2}}. \tag{1.44}$$

When the chemical potential is inside the gap, only one branch is filled, and one can verify that,

$$\sigma_H = \frac{1}{2}\frac{e^2}{h}\left(1 - \frac{m}{\sqrt{m^2+\alpha^2k_F^2}}\right) \neq 0. \tag{1.45}$$

### 2. Graphene

Graphene is probably the most famous material that has nodal points. There are two different Dirac valleys located at the corners of the hexagonal BZ. The effective Hamiltonians near the nodes are (neglecting spin)

$$\mathsf{H}_0 = \hbar v_F\left(\pm k_x\tau_x + k_y\tau_y\right), \quad \text{at } \pm K, \tag{1.46}$$

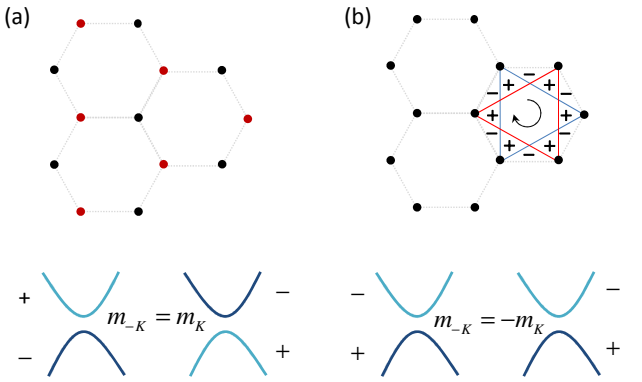


FIG. 5 (a) Graphene lattice with staggered on-site potentials opens a gap at a Dirac point, which is described by a mass. (b) A special distribution of magnetic flux invented by Haldane also opens a gap at a Dirac point, which is described by a valley-dependent mass.

where $\boldsymbol{\tau}$ is the quasi-spin for orbital degrees of freedom (i.e., conduction and valence bands), and $\pm K$ are shown in Fig. 4(a).

When an electron circles a Dirac cone once, it would get a Berry phase $\gamma_C = \pi$. According to the **Onsager quantization rule** (Chang and Niu, 1996),

$$\oint_C \mathbf{k}\cdot d\mathbf{r} = 2\pi\left(n + \frac{1}{2} - \frac{\gamma_C}{2\pi}\right). \tag{1.47}$$

The Berry phase term cancels with the 1/2, so that there is no zero-point energy for Landau levels, $\varepsilon_n = v_F\sqrt{2eB\hbar n}$. See Sec. VII.C of Xiao *et al.*, 2010 for a semiclassical derivation of the energy levels. A direct measurement of the Berry phase $\pi$ from a Dirac point in cold atoms is reported in Duca *et al.*, 2015.

Similar to the Rashba system, the Berry curvature is a delta function,

$$F_z^{\pm K} = \pm\delta^2(\mathbf{k})\tau_z. \tag{1.48}$$

Not only that the two orbitals have opposite monopole charges, the Berry curvatures of the two nodes also have opposite signs, see Fig. 4(b). As a result, the Hall conductivity is zero in the absence of magnetic field.

The *local* stability of the Dirac point in graphene is protected by space-inversion and time-reversal symmetries ($C_3$ symmetry ensures *global* stability. See Chap 7 of Bernevig and Hughes, 2013). For a staggered graphene lattice (ses Fig. 5(a)), the SIS is broken and a gap can be opened. This is described by the effective Hamiltonian,

$$\mathsf{H}^{\pm K} = \mathsf{H}_0 + mv_F^2\tau_z. \tag{1.49}$$

The Berry curvature for the lower band is

$$F_z^{\pm K}(\mathbf{k}) = \pm\frac{1}{2}\frac{k_F}{(k_F^2+k^2)^{3/2}}, \tag{1.50}$$

where $k_F = mv_F/\hbar$. The Hall conductivity remains zero, no matter where the chemical potential is, because of the cancellation from two valleys.

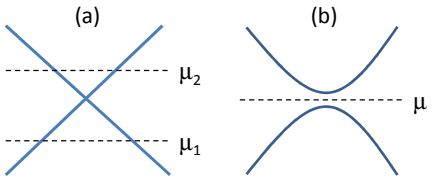


FIG. 6 (a) Dirac cone of the surface state. The chemical potential can be below ($\mu_1$) or above ($\mu_2$) the Dirac point. (b) The Dirac point can be opened by magnetization.

With an ingenious choice of flux distribution, Haldane devised a way to build two valleys with the same sign of Berry curvatures (Haldane, 1988). In Fig. 5(b), there are positive (negative) magnetic fluxes through the triangles indicated by + (−). The total flux through a hexagon is zero, thus there are no Landau levels, but the TRS is broken.

The effective Hamiltonian now becomes,

$$\mathsf{H}^{\pm K} = \mathsf{H}_0 \pm m v_F^2 \tau_z. \tag{1.51}$$

The Berry curvature for the lower band is

$$F_z^{\pm K}(\mathbf{k}) = \frac{1}{2}\frac{k_F}{(k_F^2+k^2)^{3/2}}. \tag{1.52}$$

When the chemical potential is inside the gap, the Hall conductivity is $\sigma_H = e^2/h$, because the contribution from two valleys no longer cancel with each other.

Two remarks about Haldane's graphene model : First, with proper tuning of model parameters, it's possible *not* to open the two nodes simultaneously. That is, there can be only one Dirac point, not two, at critical values. This demonstrates the **parity anomaly** in (2+1)-dimensional field theories.

Second, $\sigma_H = e^2/2h$ if there is only one gapped node. This seems to contradict the fact that the Chern number must be an integer . The half-integer here is in fact an artifact of the bottomless Dirac sea. For an usual Bloch band with lower bound, the region away from the node would contribute another 1/2 to make up for the integer. This is sometimes called a **hidden massive spectator** (see Hatsugai *et al.*, 1996).

### 3. Surface state of topological insulator

As shown in Sec. I.C, a typical TI surface state Hamiltonian near a Dirac point is

$$\mathsf{H}_{SS} = \alpha(\boldsymbol{\sigma}\times\mathbf{k})_z + O(k^2), \tag{1.53}$$

which is similar to the Rashba Hamiltonian, but without the dominant parabolic term. It has the same Berry curvature as the Rashba system,

$$F_z^{\pm} = \mp\pi\delta^2(\mathbf{k}). \tag{1.54}$$

It's not difficult to see that the Hall conductivity given by Eq. (1.42) is zero, no matter whether the chemical potential is located below or above the Dirac point (see Fig. 6(a)).

The Dirac point can be opened by magnetic dopants with magnetization $m$ (see Fig. 6(b)),

$$\mathsf{H}_{SS} = \alpha(\boldsymbol{\sigma}\times\mathbf{k})_z + m\sigma_z. \tag{1.55}$$

Same as the Rashba system, the Berry curvature is

$$F_z^{\pm} = \mp\frac{\alpha^2 m}{2(m^2+\alpha^2k^2)^{3/2}}. \tag{1.56}$$

If the chemical potential is inside the energy gap, the Hall conductivity is a half-integer,

$$\sigma_H = \frac{e^2}{h}\frac{1}{2\pi}\int d^2k F_z^- = \frac{1}{2}\frac{e^2}{h}. \tag{1.57}$$

This is different from the Rashba system. It is not a half-integer there because the lower band is not completely filled.

As we have mentioned earlier, even though the TI has odd number of Dirac point on one surface. The total number of Dirac point for all surfaces should be even. Overall they would contribute an integer Hall conductivity.

Same as in graphene, an electron circling the Fermi circle $C$ acquires a Berry phase $\gamma_C = \pi$. This value is restricted by time-reversal symmetry: If the electron circles in the opposite direction $-C$, then the Berry phase becomes $-\gamma_c$. For the graphene and the TI with TRS, we should have $\gamma_c = -\gamma_c \mod 2\pi$. Therefore, $\gamma_c$ can only be 0 or $\pi$.

Due to the phase shift of $\pi$ for a closed path, one expects to see **weak anti-localization**, instead of **weak localization**, in a graphene or a TI surface with disorders (He *et al.*, 2011). However, real samples are more complicated. Depending on condition, both types of localization can be observed (Lu and Shen, 2014; Tikhonenko *et al.*, 2009).

**Exercise**

1. Following the discussion in subsection B, generalize the effective Hamiltonian of the TI surface state to the third order of momentum,

$$\mathsf{H}(\mathbf{k}) = \varepsilon_0(k) + v_k(\sigma_x k_y - \sigma_y k_x) + \frac{\lambda}{2}\left(k_+^3 + k_-^3\right)\sigma_z. \tag{1.58}$$

2. Given the 2D Hamiltonian,

$$\mathsf{H}(\mathbf{k}) = \frac{\hbar^2k^2}{2m} + \alpha\left(\boldsymbol{\sigma}\times\mathbf{k}\right)\cdot\hat{z} + m\sigma_z, \tag{1.59}$$

show that the Berry curvature is,

$$F_z^{\pm}(\mathbf{k}) = \mp\frac{\alpha^2 m}{2(m^2+\alpha^2k^2)^{3/2}}. \tag{1.60}$$

## References


Bernevig, B. A., and T. L. Hughes, 2013, *Topological Insulators and Topological Superconductors* (Princeton University Press).

Bihlmayer, G., O. Rader, and R. Winkler, 2015, New Journal of Physics **17**(5), 050202.

Chang, M.-C., and Q. Niu, 1996, Phys. Rev. B **53**, 7010.

Culcer, D., A. MacDonald, and Q. Niu, 2003, Phys. Rev. B **68**, 045327.

Duca, L., T. Li, M. Reitter, I. Bloch, M. Schleier-Smith, and U. Schneider, 2015, **347**(6219), 288.

Fang, C., M. J. Gilbert, and B. A. Bernevig, 2013, Phys. Rev. B **87**, 035119.

Fu, L., 2009, Phys. Rev. Lett. **103**, 266801.

Haldane, F. D. M., 1988, Phys. Rev. Lett. **61**, 2015.

Hatsugai, Y., M. Kohmoto, and Y.-S. Wu, 1996, Phys. Rev. B **54**, 4898.

He, H.-T., G. Wang, T. Zhang, I.-K. Sou, G. K. L. Wong, J.-N. Wang, H.-Z. Lu, S.-Q. Shen, and F.-C. Zhang, 2011, Phys. Rev. Lett. **106**, 166805.

Kane, C., 2013, in *Topological Insulators*, edited by M. Franz and L. Molenkamp (Elsevier), volume 6 of *Contemporary Concepts of Condensed Matter Science*, pp. 3 – 34.

Lu, H.-Z., and S.-Q. Shen, 2014, Proc.SPIE **9167**, 9167.

Qi, X.-L., and S.-C. Zhang, 2011, Rev. Mod. Phys. **83**, 1057.

Tikhonenko, F. V., A. A. Kozikov, A. K. Savchenko, and R. V. Gorbachev, 2009, Phys. Rev. Lett. **103**, 226801.

Xiao, D., M.-C. Chang, and Q. Niu, 2010, Rev. Mod. Phys. **82**, 1959.

Xu, S.-Y., Y. Xia, L. A. Wray, S. Jia, F. Meier, J. H. Dil, J. Osterwalder, B. Slomski, A. Bansil, H. Lin, R. J. Cava, and M. Z. Hasan, 2011, Science **332**(6029), 560.

Zhang, H., C.-X. Liu, X.-L. Qi, X. Dai, Z. Fang, and S.-C. Zhang, 2009, Nat. Phys. **5**, 438.